Broadband tunable transmission non-reciprocity in thermal atoms dominated by two-photon transitions

Hui-Min Zhao,[1] Di-Di Zheng,[2] Xiao-Jun Zhang,[1, *] and Jin-Hui Wu[1, †]

[1]*Center for Quantum Sciences and School of Physics,*
Northeast Normal University, Changchun 130024, China
[2]*School of Mechanics and Optoelectronic Physics,*
Anhui University of Science and Technology, Huainan 232001, China
(Dated: February 12, 2024)

We propose a scheme for realizing broadband and tunable transmission non-reciprocity by utilizing two-photon near-resonant transitions in thermal atoms as single-photon far-detuned transitions can be eliminated. Our basic idea is to largely reduce the Doppler broadenings on a pair of two-photon, probe and coupling, transitions and meanwhile make the only four-photon transition Doppler-free (velocity-dependent) for a forward (backward) probe field. One main advantage of this scheme lies in that the transmission non-reciprocity can be realized and manipulated in a frequency range typically exceeding 200 MHz with isolation ratio above 20 dB and insertion loss below 1.0 dB by modulating an assistant field in frequency and amplitude. The intersecting angle between four applied fields also serves as an effective control knob to optimize the nonreciprocal transmission of a forward or backward probe field, e.g. in a much wider frequency range approaching 1.4 GHz.

I. INTRODUCTION

Nonreciprocal optical devices [1–4] permitting photon transport in one direction but not in the opposite direction, like isolators and circulators, are essential in a wide range of modern science and technology, ranging from classical light communications to quantum information processing. Though a lot of advances have been made, it is still challenging to achieve optical non-reciprocity with high isolation ratios and low insertion losses for weak light signals due to the time-reversal symmetry of most (linear) optical materials. Traditionally, magneto-optical media are used to break the time-reversal symmetry with the Faraday rotation effect, which requires however bulky magnets making against real applications involving integrated photonic devices [5–8]. Hence, significant efforts have been made recently to develop the magnet-free optical non-reciprocity by exploring different mechanisms, including nonlinear effects [9–17], spatiotemporal modulations [18–22], optomechanical interactions [23–28], moving atomic lattices [29–31], chiral quantum systems [32–36], and atomic thermal motions [37–46].

Magnet-free optical isolation exploiting thermal atoms coherently driven into the regime of electromagnetically induced transparency (EIT) is conceptually different and admirable because relevant realizations are simpler than those utilizing other mechanisms. In the typical three-level Λ configuration, for instance, the EIT response of thermal atoms may exhibit a broken time-reversal symmetry with the underlying quantum destructive interference depending critically on the propagation directions of a weak probe and a strong coupling field [37–40]. That is, a forward (backward) probe field will experience a high (low) transmissivity due to the well preserved (largely destroyed) quantum destructive interference when its two-photon resonance along with a forward coupling field is kept Doppler-free (velocity-dependent), which can be operated even at the single-photon level [46]. Such an interesting mechanism utilizing the direction-dependent interplay of EIT responses and Doppler broadenings has been extended to the four-level N configuration, exhibiting a chiral cross-Kerr nonlinear response for a probe field coming from two opposite directions [2, 40–42].

Previous studies are limited to only single-photon transitions, which can be made under appropriate conditions however negligible as compared to two-photon transitions by eliminating some intermediate states [47]. This motivates us to consider whether the direction-dependent EIT mechanism for achieving a transmission non-reciprocity, if extended to two-photon transitions [48], will provide some advantages and additional degrees of manipulation? In fact, most previous studies examine the non-reciprocal transmission of a single probe field due to limited natural linewidths of single-photon transitions, though it is possible to achieve the nonreciprocal bandwidths over 100 MHz and up to 1.0 GHz through nonlinear optical processes [42–44]. It is also known that the simultaneous manipulation of a vast number of light signals is required in all-optical networks, and wavelength division multiplexing (WDM) [49–51] is an effective technique for enlarging the information capacity of optical fiber communication [52–57]. Then, a specific question arises, whether the linear non-reciprocal transmission, if extended to systems dominated by two-photon transitions, can be realized in a wide enough frequency range appropriate for the WDM manipulation of multiple probe fields?

With above considerations, here we investigate a five-level Λ system for achieving two-photon EIT responses sensitive to the propagating direction of a probe field as it can be reduced to a three-level Λ system with two inter-

mediate states being adiabatically eliminated. This is attained by making a probe and an assistant field as well as two coupling fields to keep two-photon near resonance, respectively, when the two pairs of oppositely propagating fields are far detuned from relevant single-photon transitions. Taking thermal atoms into account, we find that the probe field incident upon one side exhibits very low losses while that upon the other side is strongly absorbed in a frequency range of tens of natural linewidths (> 200 MHz) controlled by the assistant field. This broadband transmission non-reciprocity, facilitating WDM, of high isolation ratios (> 20 dB) and low insertion losses (< 1.0 dB) is a result of the direction-dependent Doppler effect on the only four-photon transition and the largely reduced Doppler broadenings on both two-photon transitions. It is also of interest that the intersecting angle between the two pairs of oppositely traveling fields can be tuned to realize a broader nonreciprocal bandwidth (i.e., up to 1.4 GHz for instance).

II. MODEL & EQUATIONS

We consider in Fig. 1(a) a five-level atomic system coherently driven into the Λ configuration with two lower ground states $|1\rangle$ and $|2\rangle$, two intermediate excited states $|3\rangle$ and $|4\rangle$, and an upper excited state $|5\rangle$. A probe field of frequency ω_p (amplitude E_p), an assistant field of frequency ω_a (amplitude E_a), a first coupling field of frequency ω_{c1} (amplitude E_{c1}) and a second coupling field of frequency ω_{c2} (amplitude E_{c2}) act upon four transitions $|1\rangle \leftrightarrow |3\rangle$, $|3\rangle \leftrightarrow |5\rangle$, $|2\rangle \leftrightarrow |4\rangle$, and $|4\rangle \leftrightarrow |5\rangle$, respectively. The corresponding (real) Rabi frequencies are $\Omega_p = d_{13}E_p/2\hbar$, $\Omega_a = d_{35}E_a/2\hbar$, $\Omega_{c1} = d_{24}E_{c1}/2\hbar$, and $\Omega_{c2} = d_{45}E_{c2}/2\hbar$, respectively, with d_{mn} being electric dipole moment on transition $|m\rangle \leftrightarrow |n\rangle$. In addition, we have defined $\Delta_p = \omega_p - \omega_{31}$ and $\Delta_a = \omega_a - \omega_{53}$ as single-photon detunings on the two left-arm transitions while $\Delta_{c1} = \omega_{c1} - \omega_{42}$ and $\Delta_{c2} = \omega_{c2} - \omega_{54}$ as single-photon detunings on the two right-arm transitions. Then, in the electric-dipole and rotating-wave approximations, we can write down the interaction Hamiltonian

$$H_I = -\hbar \begin{pmatrix} 0 & 0 & \Omega_p^* & 0 & 0 \\ 0 & \Delta_{12} & 0 & \Omega_{c1}^* & 0 \\ \Omega_p & 0 & \Delta_{13} & 0 & \Omega_a^* \\ 0 & \Omega_{c1} & 0 & \Delta_{14} & \Omega_{c2}^* \\ 0 & 0 & \Omega_a & \Omega_{c2} & \Delta_{15} \end{pmatrix}, \quad (1)$$

with $\Delta_{12} = \Delta_p + \Delta_a - \Delta_{c1} - \Delta_{c2}$, $\Delta_{13} = \Delta_p$, $\Delta_{14} = \Delta_p + \Delta_a - \Delta_{c2}$, and $\Delta_{15} = \Delta_p + \Delta_a$.

In the present work, we are only interested in the parametric regions where single-photon detunings and Rabi frequencies are so carefully chosen that two-photon near-resonant transitions $|1\rangle \leftrightarrow |5\rangle$ and $|2\rangle \leftrightarrow |5\rangle$ are dominant over single-photon far-detuned transitions $|1\rangle \leftrightarrow |3\rangle$, $|3\rangle \leftrightarrow |5\rangle$, $|2\rangle \leftrightarrow |4\rangle$, and $|4\rangle \leftrightarrow |5\rangle$. This indicates that the five-level Λ system in Fig. 1(a) can be reduced to the

three-level Λ system in Fig. 1(b) under appropriate conditions, allowing us to simplify relevant calculations on one hand and explore new physics on the other hand. To be more specific, in the case of $\Delta_p + \Delta_a \simeq 0$, $\Delta_{c1} + \Delta_{c2} \simeq 0$, $|\Delta_{p,a}| \gg \Omega_{p,a}$, and $|\Delta_{c1,c2}| \gg \Omega_{c1,c2}$, it is viable to derive via the time-averaged adiabatic-elimination method [48] the effective interaction Hamiltonian

$$H_e = -\hbar \begin{pmatrix} 0 & 0 & \Omega_{pe}^* \\ 0 & \Delta_{12} + \Delta_{2d} & \Omega_{ce}^* \\ \Omega_{pe} & \Omega_{ce} & \Delta_{15} + \Delta_{5d} \end{pmatrix}, \quad (2)$$

where we have introduced a new Rabi frequency $\Omega_{pe} = -\Omega_p\Omega_a/\Delta_p$ ($\Omega_{ce} = -\Omega_{c1}\Omega_{c2}/\Delta_{c2}$) for the effective probe (coupling) field of frequency $\omega_{pe} = \omega_p + \omega_a$ ($\omega_{ce} = \omega_{c1} + \omega_{c2}$) acting upon the two-photon near-resonant transition $|1\rangle \leftrightarrow |5\rangle$ ($|2\rangle \leftrightarrow |5\rangle$). Note also that $\Delta_{2d} \simeq -|\Omega_{c1}|^2/\Delta_{c1}$ ($\Delta_{5d} \simeq |\Omega_a|^2/\Delta_a + |\Omega_{c2}|^2/\Delta_{c2}$) describes the dynamic Stark shift of state $|2\rangle$ ($|5\rangle$) as a direct result of the virtual absorption and emission of ω_{c1} (ω_a and ω_{c2}) photons, which will result in a slight deviation of the four-photon (two-photon) resonance from $\Delta_{12} = 0$ ($\Delta_{15} = 0$). The validity for eliminating states $|3\rangle$ and $|4\rangle$ can be verified by comparing probe absorption spectra obtained by solving dynamic equations for the five-level Λ system starting from Eq. (1) and those for the three-level Λ system starting from Eq. (2) (see the Appendix A).

For simplicity, here we just write down dynamic equations for the reduced three-level Λ system with respect to density matrix element ρ_{mn} referring to atomic population ($m = n$) or coherence ($m \neq n$) [58]

$$\partial_t \rho_{22} = \Gamma_{52}\rho_{55} + i\Omega_{ce}^*\rho_{52} - i\Omega_{ce}\rho_{25}, \quad (3a)$$

$$\partial_t \rho_{11} = \Gamma_{51}\rho_{55} + i\Omega_{pe}^*\rho_{51} - i\Omega_{pe}\rho_{15}, \quad (3b)$$

$$\partial_t \rho_{52} = -g_{52}\rho_{52} + i\Omega_{pe}\rho_{12} + i\Omega_{ce}(\rho_{22} - \rho_{55}), \quad (3c)$$

$$\partial_t \rho_{51} = -g_{51}\rho_{51} + i\Omega_{ce}\rho_{21} + i\Omega_{pe}(\rho_{11} - \rho_{55}), \quad (3d)$$

$$\partial_t \rho_{21} = -g_{21}\rho_{21} + i\Omega_{ce}^*\rho_{51} - i\Omega_{pe}\rho_{25}, \quad (3e)$$

which are restricted by $\rho_{ij} = \rho_{ji}^*$ and $\rho_{11} + \rho_{22} + (1 + \eta_{53} + \eta_{54})\rho_{55} = 1$ with $\eta_{53}\rho_{55} = \Gamma_{53}/(\Gamma_{31} + \Gamma_{32})\rho_{55}$ and $\eta_{54}\rho_{55} = \Gamma_{54}/(\Gamma_{41} + \Gamma_{42})\rho_{55}$ accounting for populations in states $|3\rangle$ and $|4\rangle$, respectively, due to the inevitable spontaneous decay. Above, we have defined the complex decoherence rates $g_{52} = \gamma_{52} + i(\Delta_{15} - \Delta_{12} + \Delta_{5d} - \Delta_{2d})$, $g_{51} = \gamma_{51} - i(\Delta_{15} + \Delta_{5d})$ and $g_{21} = \gamma_{21} - i(\Delta_{12} + \Delta_{2d})$ after including the dynamic Stark shifts Δ_{2d} and Δ_{5d}. Typically, the real dephasing rate γ_{mn} of coherence ρ_{mn} depends on the spontaneous decay rates Γ_{mk} and Γ_{nk} of populations ρ_{mm} and ρ_{nn} through $\gamma_{mn} = \sum_k(\Gamma_{mk} + \Gamma_{nk})/2$. We have also defined $\Gamma_{51} = \Gamma_{31}\eta_{53} + \Gamma_{41}\eta_{54}$ and $\Gamma_{52} = \Gamma_{32}\eta_{53} + \Gamma_{42}\eta_{54}$ as the effective decay rates from state $|5\rangle$ to states $|1\rangle$ and $|2\rangle$, respectively.
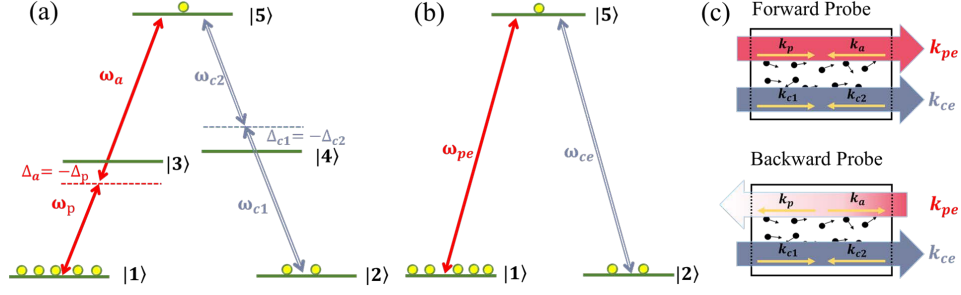
FIG. 1. (a) An original five-level Λ system driven by a probe field ω_p, an assistant field ω_a, and two coupling fields $\omega_{c1,c2}$ set with large single-photon detunings while in appropriate two-photon resonances. (b) An equivalent three-level Λ system driven by an effective probe field $\omega_{pe} = \omega_p + \omega_a$ and an effective coupling field $\omega_{ce} = \omega_{c1} + \omega_{c2}$ on different two-photon transitions. (c) An illustration of nonreciprocal light propagation in a warm atomic sample for counter-traveling probe fields with wavevectors k_p and $-k_p$, respectively. Other fields have been arranged to largely reduce Doppler broadenings on both two-photon transitions with effective probe $\pm k_{pe} = \pm(k_p - k_a)$ and coupling $k_{ce} = k_{c1} - k_{c2}$ wavevectors.

In the limit of a weak effective probe field ($\Omega_{pe} \to 0$), solving Eqs. (3) by setting $\partial_t \rho_{mn} = 0$, we can obtain the steady-state atomic population in state $|5\rangle$

$$\rho_{55} = \frac{2\gamma |\Omega_{pe}|^2 \Delta_{12e}^2 / \Gamma}{|\Omega_{ce}|^4 - 2|\Omega_{ce}|^2 \Delta_{12e}\Delta_{15e} + (\Gamma^2 + \Delta_{15e}^2)\Delta_{12e}^2}, \quad (4)$$

with $\Delta_{12e} = \Delta_{12} + \Delta_{2d}$ and $\Delta_{15e} = \Delta_{15} + \Delta_{5d}$ being effective detunings on transitions $|1\rangle \leftrightarrow |2\rangle$ and $|1\rangle \leftrightarrow |5\rangle$, respectively. We have also considered $\Gamma_{51} = \Gamma_{52} = \Gamma$ for appropriate atomic states and $\gamma_{51} = \gamma_{52} = \Gamma + \gamma_l$ with γ_l being the common linewidth of all laser fields while neglecting the much smaller decoherence rate γ_{21} arising from atomic collisions. Then it is viable to further obtain the absorption coefficient and the probe transmissivity (see the Appendix A) as given below

$$\alpha_p = \frac{N d_{13}^2}{\hbar \varepsilon_0} \frac{\pi \Gamma}{\lambda_p} \frac{\rho_{55}}{|\Omega_p|^2}, \quad (5a)$$

$$T_p = e^{-\alpha_p L}, \quad (5b)$$

where N (L) denotes the density (length) of a cold atomic sample while λ_p is the wavelength of a weak probe field traveling through this atomic sample.

Taking a thermal atomic sample into account, frequencies of the probe, assistant, and two coupling fields will be shifted to different extents for a certain Maxwell distribution of atomic velocity v depending on their propagating directions, yielding thus different Doppler effects. We have a total of sixteen geometric arrangements for the four applied fields as they propagate along either the z or the $-z$ direction, two among which, referred to as the cases of (i) forward and (ii) backward probes, are of our special interest as shown in Fig. 1(c). In both cases, the probe and assistant fields as well as the two coupling fields have been arranged to propagate in the opposite directions so as to well suppress the Doppler broadenings on two-photon transitions $|1\rangle \leftrightarrow |5\rangle$ and $|2\rangle \leftrightarrow |5\rangle$. To be

more specific, the single-photon detunings should be replaced by $\Delta_p + k_p v$, $\Delta_a - k_a v$, $\Delta_{c1} + k_{c1} v$, and $\Delta_{c2} - k_{c2} v$ in case (i) while by $\Delta_p - k_p v$, $\Delta_a + k_a v$, $\Delta_{c1} + k_{c1} v$, and $\Delta_{c2} - k_{c2} v$ in case (ii) with '+' and '−' denoting the z and $-z$ directions, respectively. Here we have introduced wavenumbers $k_i = 2\pi/\lambda_i$ and wavelengths λ_i for relevant light fields with $i \in \{p, a, c1, c2\}$. Accordingly, the two-photon detunings should be replaced by $\Delta_{15} + k_{pe} v$ and $\Delta_{15} - \Delta_{12} + k_{ce} v$ in case (i) while by $\Delta_{15} - k_{pe} v$ and $\Delta_{15} - \Delta_{12} + k_{ce} v$ in case (ii) with largely reduced effective wavevectors $k_{pe} = k_p - k_a$ and $k_{ce} = k_{c1} - k_{c2}$, which must result in well suppressed Doppler broadenings on two-photon transitions. On the other hand, the four-photon detuning should be replaced by $\Delta_{12} + (k_{pe} - k_{ce})v$ in case (i) while by $\Delta_{12} - (k_{pe} + k_{ce})v$ in case (ii). Hence, it is Doppler-free and velocity-dependent, respectively, in cases (i) and (ii) due to $k_{pe} = k_{ce}$ with $k_p = k_{c1}$ and $k_a = k_{c2}$, which is crucial for realizing the transmission non-reciprocity of a weak probe field.

With above considerations, it is viable to calculate the mean populations in state $|5\rangle$ by making following integrations for the two cases of our interest

$$\rho_{55}^{\pm} = \int dv f(v) \rho_{55}(\pm k_p v; \mp k_a v; k_{c1} v, -k_{c2} v), \quad (6)$$

where $f(v) = e^{-v^2/v_p^2}/(v_p\sqrt{\pi})$ denotes the Maxwell velocity distribution with $v_p = \sqrt{2k_B T/M}$ being the most probable atomic velocity, k_B the Boltzmann constant, T the atomic temperature, and M the atomic mass. With $\rho_{55}^{\pm}$ in hand, we can further calculate the absorption coefficients and the probe transmissivities via

$$\alpha_p^{\pm} = \frac{N d_{13}^2}{\hbar \varepsilon_0} \frac{\pi \Gamma}{\lambda_p} \frac{\rho_{55}^{\pm}}{|\Omega_p|^2}, \quad (7a)$$

$$T_p^{\pm} = e^{-\alpha_p^{\pm} L}, \quad (7b)$$

which should be direction-dependent due to $\rho_{55}^+ \neq \rho_{55}^-$. In addition to the qualitative evaluations via $T_p^+ \neq T_p^-$,

the transmission non-reciprocity for a probe field can also be quantified via two figure of merits

$$\mathtt{IR} = 10 \log_{10} \left(\frac{T_p^+}{T_p^-} \right), \tag{8a}$$

$$\mathtt{IL} = -10 \log_{10} T_p^+, \tag{8b}$$

referring to isolation ratio and insertion loss, respectively. Here we have considered that $T_p^+ \gg T_p^-$ around the four-photon resonance $\Delta_{12} + \Delta_{2d} = 0$ where a two-photon EIT window can be found in case (i) due to the Doppler-free arrangement but is smeared out in case (ii) by the residual Doppler effect. Below, we will adopt $\mathtt{IR} > 20$ dB (i.e., $T_p^+/T_p^- > 100$) and $\mathtt{IL} < 1.0$ dB (i.e., $T_p^+ > 0.794$) as two basic criteria for realizing a high-performance isolator based on the transmission non-reciprocity.

It is worth noting that, effective Rabi frequencies and dynamic Stark shifts in the reduced three-level Λ system are also velocity-dependent as shown below

$$\Omega_{pe}^{\pm} = -\frac{\Omega_p \Omega_a}{\Delta_p \pm k_p v}, \tag{9a}$$

$$\Omega_{ce}^{\pm} = -\frac{\Omega_{c1} \Omega_{c2}}{\Delta_{c2} - k_{c2} v}, \tag{9b}$$

$$\Delta_{2d}^{\pm} = -\frac{|\Omega_{c1}|^2}{\Delta_{c1} + k_{c1} v}, \tag{9c}$$

$$\Delta_{5d}^{\pm} = \frac{|\Omega_a|^2}{\Delta_a \mp k_a v} + \frac{|\Omega_{c2}|^2}{\Delta_{c2} - k_{c2} v}, \tag{9d}$$

which may destroy the two-photon EIT effect in case (i). Fortunately, their values are very small and more importantly change little for most atomic velocities even at a room temperature as we choose large enough $|\Delta_{p,a,c1,c2}|$. Last but not least, the assistant (second coupling) field may intersect the oppositely propagating probe (first coupling) field with a misaligned angle $180° - \theta$ while the latter is kept to always travel along the $\pm z$ (z) direction with '+' and '−' referring to cases (i) and (ii), respectively. Then, wavevectors $k_{a,c2}$ should be replaced with the effective ones $k_{a,c2}^{\mathtt{eff}} = k_{a,c2} \cos(180° - \theta)$ in calculating $\rho_{55}^{\pm}$. The velocity-insensitive $\{\Omega_{pe,ce}^{\pm}, \Delta_{2d,5d}^{\pm}\}$ and angle-dependent $k_{a,c2}^{\mathtt{eff}}$ can be explored to bring additional degrees of dynamic manipulation on the transmission non-reciprocity discussed in the next two sections.

III. BROADBAND NON-RECIPROCITY

In this section, we examine via numerical calculations the broadband transmission non-reciprocity of a probe field incident upon a sample of thermal atoms driven into the five-level Λ configuration in Fig. 1(a) equivalent to the three-level Λ configuration in Fig. 1(b) under appropriate conditions. We will consider ^{87}Rb atoms as an example with states $|1\rangle = |5S_{1/2}, F = 1\rangle$, $|2\rangle = |5S_{1/2}, F = 2\rangle$, $|3\rangle = |5P_{1/2}, F = 1\rangle$, $|4\rangle = |5P_{1/2}, F = 2\rangle$, and $|5\rangle = |7S_{1/2}, F = 2\rangle$, exhibiting transition wavelengths $\lambda_p = \lambda_{c1} = 795.0$ nm and $\lambda_a = \lambda_{c2} = 728.7$ nm as well as decay rates $\Gamma_{31} = \Gamma_{32} = \Gamma_{41} = \Gamma_{42} = 5.75$ MHz and $\Gamma_{53} = \Gamma_{54} = 0.19$ MHz [59, 60]. The half Doppler broadenings can be estimated by $\delta\omega_D = \sqrt{\ln 2} v_p / \lambda_i$ and are about 250 (274) MHz on the lower (upper) single-photon transitions with $i \in \{p, c1\}$ ($i \in \{a, c2\}$) but reduced to 22.8 MHz on the two-photon transitions with $i \in \{pe, ce\}$ at the temperature $T \simeq 300$ K ($v_p \simeq 240$ m/s). It is hence appropriate to choose $\Delta_{a,c1}/ \simeq -\Delta_{p,c2} \simeq 1000$ MHz and $\Omega_{a,c1,c2} \lesssim 50$ MHz so that the single-photon transitions can be neglected for all atomic velocities while the two-photon transitions are kept near resonances by setting $\Delta_{15} \simeq 0$ and $\Delta_{15} - \Delta_{12} - \Delta_{12d} \simeq 0$ with Δ_{12d} being small and Δ_{15d} negligible (due to $\Delta_a = -\Delta_{c2}$).

In Fig. 2, we plot two-photon absorption coefficients $\alpha_p^{\pm}$ as functions of probe detuning Δ_p for three typical temperatures spanning a wide range. We can see from Figs. 2(a$_1$,a$_2$) that there exist no observable differences between α_p^+ and α_p^- at a low enough temperature $T = 1.0$ mK, leaving the cold atomic sample reciprocal in absorption to a weak probe field incident from the left or right side. Moreover, it is clear that each absorption spectrum of α_p^+ and α_p^- on the two-photon transition $|1\rangle \leftrightarrow |5\rangle$ exhibits a typical EIT doublet with an in-between dip at $\Delta_p \simeq -\Delta_a$, which can be attributed to the quantum destructive interference generated by an effective coupling field Ω_{ce} acting upon the two-photon transition $|2\rangle \leftrightarrow |5\rangle$. As the temperature increases to $T = 10$ K in Figs. 2(b$_1$,b$_2$) or to $T = 300$ K in Figs. 2(c$_1$,c$_2$), we find that α_p^+ and α_p^- become evidently different around $\Delta_p \simeq -\Delta_a$ where the two-photon EIT dips remain unchanged in depth, though become narrower, for α_p^+ but entirely disappear for α_p^-. The underlying physics is related to the four-photon detunings

$$\Delta_{12}^{\pm} = \Delta_{12} + (k_{ep} \mp k_{ec}) v - \Delta_{2d}^{\pm}, \tag{10}$$

for $\alpha_p^{\pm}$ with $\Delta_{2d}^+ = \Delta_{2d}^-$ depending on but insensitive to v. This equation indicates that α_p^+ is roughly Doppler-free around $\Delta_{12} = 0$ due to $k_{ep} - k_{ec} = 0$ so that the EIT window remains perfect while α_p^- is velocity-dependent everywhere due to $k_{ep} + k_{ec} = 2k_{ep}$ so that the EIT window entirely disappears. It is worth noting that the increase of $\alpha_p^{\pm}$ with Ω_{pe} observed for all three temperatures is a feature absent in the three-level Λ system dominated by single-photon transitions and will be used later to manipulate the transmission non-reciprocity.

Above results indicate that the forward probe field can exhibit a rather high transmissivity, while the backward probe field will be strongly absorbed, around the four-photon resonance $\Delta_p + \Delta_a \simeq \Delta_{c1} + \Delta_{c2}$ in a sample of thermal atoms described by $\alpha_p^{\pm}$. Such an evident transmission non-reciprocity, enabling an efficient optical isolation, has been numerically examined in Fig. 3 in terms
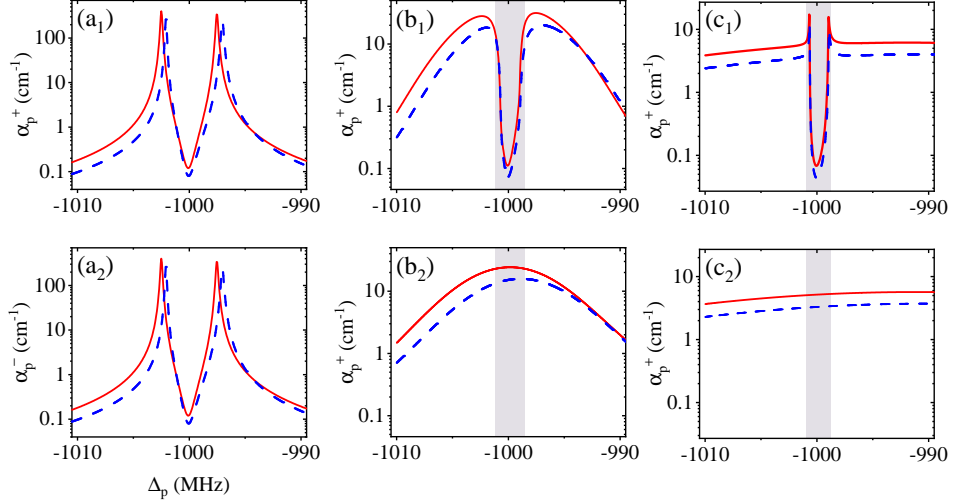
FIG. 2. Absorption coefficients α_p^+ (upper) and α_p^- (lower) as functions of probe detuning Δ_p with $T = 1.0$ mK (a_1,a_2), 10 K (b_1,b_2), and 300 K (c_1,c_2) for $\Omega_a = 50$ MHz (red-solid) and 40 MHz (blue-dashed). Other parameters are $\Omega_p = 0.1$ MHz, $\Omega_{c1} = \Omega_{c2} = 50$ MHz, $\Delta_a = \Delta_{c1} = 1000$ MHz, $\Delta_{c2} = -1002.5$ MHz, $\Gamma = 0.19$ MHz, $\gamma_l = 0.05$ MHz, $\gamma_{21} = 2.0$ kHz, $\theta = 180°$, $N = 2.0 \times 10^{12}$ cm^{-3}, $L = 1.0$ cm, $\lambda_p = 795.0$ nm, and $d_{13} = 2.537 \times 10^{-29}$ Cm.
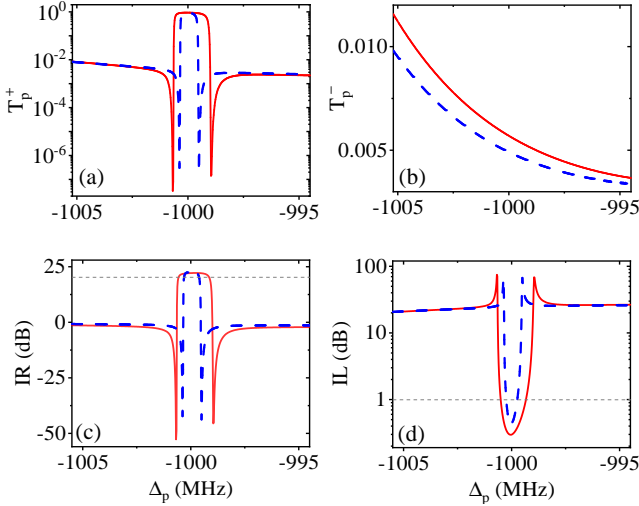
FIG. 3. Probe transmissivities T_p^+ (a) and T_p^- (b) as well as isolation ratio IR (c) and insertion loss IL (d) against probe detuning Δ_p for $\Omega_{c1} = \Omega_{c2} = 50$ MHz (red-solid) and 40 MHz (blue-dashed). Other parameters are the same as in Fig. 2 except $T = 300$ K and $\Omega_a = 50$ MHz. Gray dotted lines refer to IR = 20 dB in (c) or IL = 1.0 dB in (d) as a reference.

mum of 22.5 dB while IL might be as low as 0.3 dB, indicating the possibility for achieving a high-performance optical isolator. Note however that the effective coupling Rabi frequency Ω_{ce} should not be too small, otherwise the insertion loss will exceed 1.0 dB on one hand and the non-reciprocal transmission bandwidth will reduce to be invisible on the other hand (not shown).
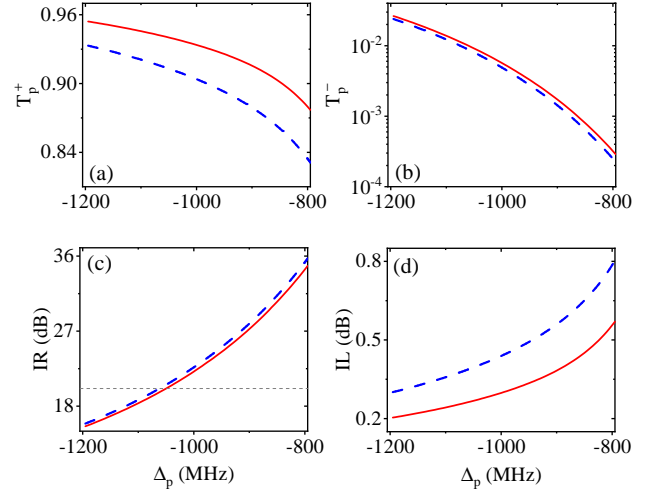

FIG. 4. Probe transmissivities T_p^+ (a) and T_p^- (b) as well as isolation ratio IR (c) and insertion loss IL (d) against probe detuning Δ_p for $\Omega_{c1} = \Omega_{c2} = 50$ MHz (red-solid) and 40 MHz (blue-dashed). Other parameters are the same as in Fig. 3 except $\Delta_a = -\Delta_p$. Gray dotted lines refer to IR = 20 dB in (c) or IL = 1.0 dB in (d) as a reference.

of transmissivities $T_p^\pm$, isolation ratio IR, and insertion loss IL as functions of probe detuning Δ_p. We find from Fig. 3(a) that T_p^+ approaches unity with a transmission bandwidth of the order of MHz determined here by the effective coupling Rabi frequency Ω_{ce} while Fig. 3(b) shows that T_p^- remains low in a much wider range though decreases slowly as $|\Delta_p|$ becomes smaller due to an increase of the effective probe Rabi frequency Ω_{pe}. It is also clear from Fig. 3(c) and 3(d) that IR could reach the maxi-

We are committed in particular to achieving the non-reciprocal transmission of a controlled broad bandwidth

based on thermal atoms dominated by two-photon transitions under consideration here. Working in the regime of near-resonant two-photon and four-photon transitions, the single-photon detunings can be tuned in a relatively wide range yet without changing too much the four important quantities plotted in Fig. 4, which then facilitates the essential WDM function in an all-optical network. This has been examined by modulating $\Delta_p = -\Delta_a$ in the range of $\{-1200, -800\}$ MHz to ensure that two-photon transitions are dominant over single-photon transitions. In this range, it is found that slight changes of effective Rabi frequency Ω_{pe} has resulted in the evident changes in $T_p^{\pm}$, IR, and IL, which is impossible in a typical three-level Λ system. More importantly, Fig. 4 shows that the isolation ratio of IR > 20 dB and the insertion loss of IL < 1.0 dB can be attained in a wide frequency range of $150 \sim 250$ MHz, indicating that it is viable to achieve the nonreciprocal transmission by simultaneously handling tens of light signals with different frequencies. Fig. 5 further shows that the nonreciprocal transmission exhibits a maximal bandwidth up to 1.4 GHz with IR > 20 and IL < 1.0 dB as we choose $\theta = 158°$ so as to have the smallest Doppler broadenings on both two-photon transitions $|1\rangle \leftrightarrow |5\rangle$ and $|2\rangle \leftrightarrow |5\rangle$. This big enlargement of nonreciprocal bandwidth can be understood by resorting to numerical results shown in the next section.
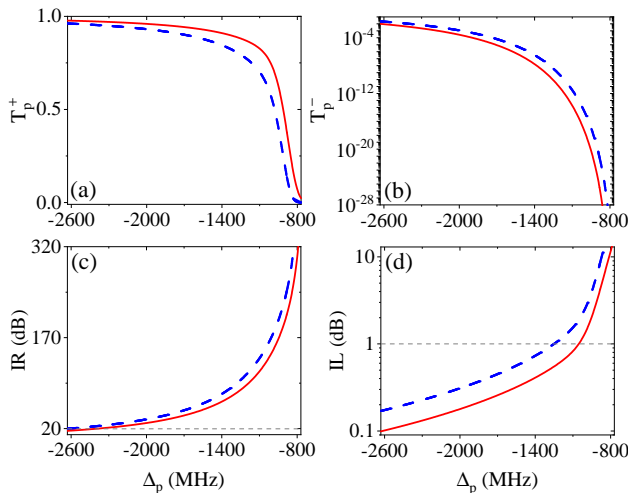

FIG. 5. Probe transmissivities T_p^+ (a) and T_p^- (b) as well as isolation ratio IR (c) and insertion loss IL (d) against probe detuning Δ_p for $\Omega_{c1} = \Omega_{c2} = 50$ MHz (red-solid) and 40 MHz (blue-dashed). Other parameters are the same as in Fig. 4 except $\theta = 158°$. Gray dotted lines refer to IR = 20 dB in (c) or IL = 1.0 dB in (d) as a reference.

IV. NONRECIPROCAL TUNABILITY

In this section, we examine two flexible ways for manipulating the transmission non-reciprocity by modulating additional parameters, Rabi frequency Ω_a and misaligned

angle θ, to gain further insights into nonreciprocal optical responses. This is intrinsic to the reduced three-level Λ system dominated by two-photon near-resonant transitions and expected to facilitate the signal or information processing in an all-optical network.

First, we plot in Fig. 6 probe transmissivities $T_p^{\pm}$ together with isolation ratio IR and insertion loss IL against Rabi frequency Ω_a of the assistant field. It is easy to see from Figs. 6(a) and 6(b) that a large variation of Ω_a in the range of $\{0, 60\}$ MHz, corresponding to a small variation of Ω_{pe} in the range of $\{0, 6\}$ kHz, will result in the evident variations of $T_p^{\pm}$, which cannot be attained in a typical three-level Λ system independent of probe Rabi frequency Ω_p. We should note, however, that T_p^+ just reduces a few percentage from 1.0 to 0.90 or 0.86 (depending on coupling Rabi frequencies $\Omega_{c1} = \Omega_{c2}$) while T_p^- suffers a much sharper reduction from 1.0 to 5×10^{-4} or 4×10^{-4} (less sensitive to the change of $\Omega_{c1} = \Omega_{c2}$). Accordingly, we find from Figs. 6(c) and 6(d) that isolation ratio IR increases faster than insertion loss IL with the increase of Ω_a, and we can achieve IR > 20 dB only with $\Omega_a > 47.5$ MHz ($\Omega_a > 47.0$ MHz) while IL < 1.0 dB holds for $\Omega_a \leq 60$ MHz no matter $\Omega_{c1} = \Omega_{c2} = 50$ MHz or $\Omega_{c1} = \Omega_{c2} = 40$ MHz. It is also clear that the assistant field should be carefully modulated in order to ensure an ideal trade-off between IR and IL, relevant to a high-performance optical isolator, with the working range of Ω_a depending on $\Omega_{c1} = \Omega_{c2}$ for a fixed Ω_p.
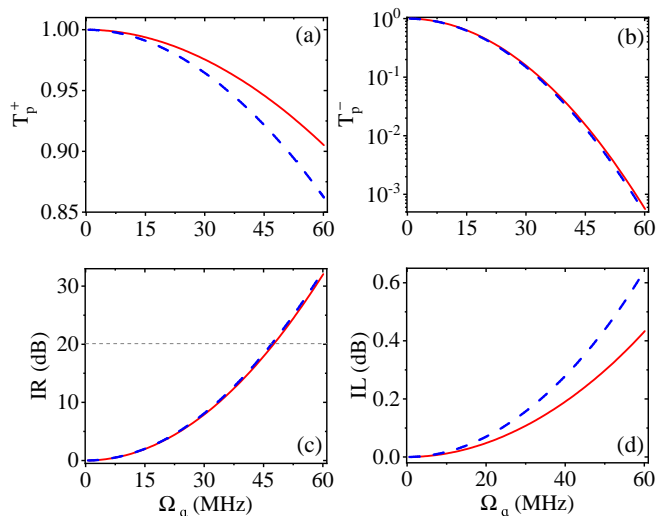

FIG. 6. Probe transmissivities T_p^+ (a) and T_p^- (b) as well as isolation ratio IR (c) and insertion loss IL (d) against Rabi frequency Ω_a for $\Omega_{c1} = \Omega_{c2} = 50$ MHz (red-solid) and 40 MHz (blue-dashed). Other parameters are the same as in Fig. 3 except $\Delta_p = -1000$ MHz. Gray dotted lines refer to IR = 20 dB in (c) or IL = 1.0 dB in (d) as a reference.

Then, we try to plot in Fig. 7 probe transmissivities $T_p^{\pm}$ together with isolation ratio IR and insertion loss IL against misaligned angle θ between wavenumbers k_p (k_{c1}) and $-k_a$ ($-k_{c2}$) in the case of $\Delta_p = -\Delta_a$. Fig. 7(a)

shows that T_p^+ decreases slowly above a quite high value until θ reduces from $180°$ to $157.3°$, while approaches quickly 4×10^{-3} (5×10^{-6}) for $\Omega_{c1} = \Omega_{c2} = 50$ MHz ($\Omega_{c1} = \Omega_{c2} = 40$ MHz) as θ further reduces from $157.3°$ to $156.5°$. Fig. 7(b) shows instead that T_p^- exhibits an extremely small minimum around $\theta = 157.3°$, decreases more evidently as θ reduces from $180°$ to $157.3°$, and increases surprisingly back to 1.0 as θ further reduces from $157.3°$ to $156.5°$. The joint variations of T_p^+ and T_p^- due to a simple modulation of angle θ then lead to the results shown in Fig. 7(c) and 7(d), where IR exhibits a very large maximum at $\theta = 157.3°$ while IL increases continuously to a saturation value as θ reduces to $156.5°$. It is worth noting that the critical requirements of IR > 20 dB and IL < 1.0 dB could be simultaneously attained only with $\theta > 158.6°$ ($\theta > 160.3°$) for $\Omega_{c1} = \Omega_{c2} = 50$ MHz ($\Omega_{c1} = \Omega_{c2} = 40$ MHz), while the maximum of IR at $\theta = 157.3°$ is meaningless as the corresponding IL is too large. Anyway, we can get a better trade-off between IR and IL for realizing a high-performance optical isolation by modulating θ in the range of $\{157.3°, 180°\}$.

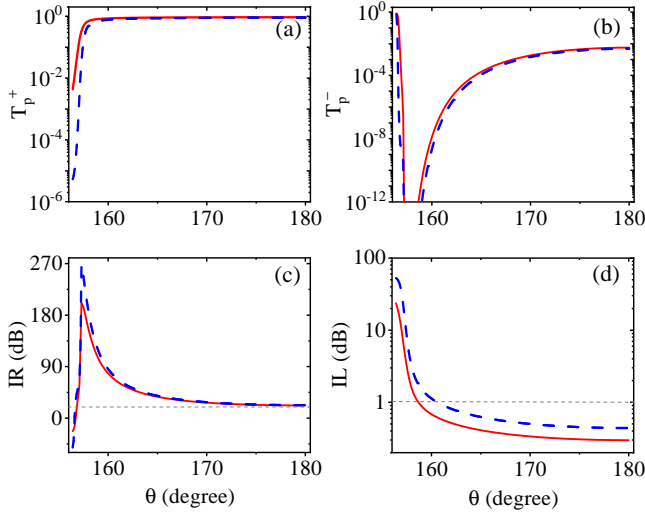FIG. 7. Probe transmissivities T_p^+ (a) and T_p^- (b) as well as isolation ratio IR (c) and insertion loss IL (d) against angle θ for $\Omega_{c1} = \Omega_{c2} = 50$ MHz (red-solid) and 40 MHz (blue-dashed). Other parameters are the same as in Fig. 3 except $\Delta_p = -1000$ MHz. Gray dotted lines refer to IR = 20 dB in (c) or IL = 1.0 dB in (d) as a reference.

To better understood what are observed in Fig. 7, we examine in Fig. 8 absorption coefficients $\alpha_p^\pm$ as functions of probe detuning Δ_p for three typical values of angle θ. Fig. 8(a) shows that the EIT window of α_p^+ becomes shallower and shallower and meanwhile more and more asymmetric as θ gradually reduces. Fig. 8(b) shows that α_p^- changes in a way similar to α_p^+ as far as their spectral widths are concerned, $i.e.$ both become narrower as θ gradually reduces. An evident change of α_p^- different from α_p^+ lies in that the two-photon EIT dip is absent for both $\theta = 180°$ and $\theta = 160°$ but can be observed like

α_p^+ for $\theta = 156.5°$. This can be understood by considering that $\theta = 156.5°$ corresponds to the case where both two-photon transitions $|1\rangle \leftrightarrow |5\rangle$ and $|2\rangle \leftrightarrow |5\rangle$ become Doppler free due to $k_{p,c1} = k_{a,c2}^{\text{eff}}$ so that it is impossible to attain the transmission non-reciprocity around four-photon resonance without residual Doppler broadenings. As to the asymmetric features of α_p^+ and α_p^- spectra, they arise in fact from effective Rabi frequencies $\Omega_{pe}^\pm$ and $\Omega_{ce}^\pm$ as well as dynamic Stark shifts $\Delta_{2d}^\pm$ and $\Delta_{5d}^\pm$, whose velocity dependence cannot be eliminated via appropriate arrangements of the probe, assistant, and coupling fields. Fortunately, the four quantities exhibit quite small values and change just a little for different atomic velocities so that the EIT dip remains well developed. With above discussions, we conclude that the quenching of T_p^+ for $\theta < 157.3°$ and the minimum of T_p^- at $\theta = 157.3°$ in Fig. 7 arise from the Doppler-free asymmetric EIT spectra of $\alpha_p^\pm$ and a slight velocity-dependent shift of the EIT dip away from four-photon resonance.
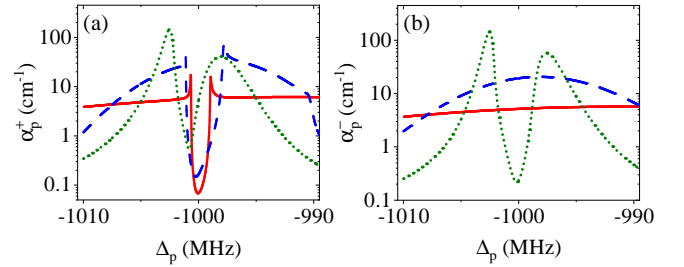

FIG. 8. Absorption coefficients α_p^+ (a) and α_p^- (b) as functions of probe detuning Δ_p for $T = 300$ K with $\theta = 180°$ (red-solid), $160°$ (blue-dashed), and $156.5°$ (green-dotted). Other parameters are the same as in Fig. 3.

What we observe in Fig. 7 and Fig. 8 answer why the nonreciprocal bandwidth can be greatly enlarged by replacing $\theta = 180°$ with $\theta = 158°$ at $T = 300$ K as shown in Fig. 5. Finally, we examine in Fig. 9 the joint effects of angle θ and temperature T on the transmission non-reciprocity in terms of isolation ratio IR and insertion loss IL in the case of $\Delta_p = -\Delta_a$. We can see that there is an optimal temperature where IR exhibits a maximum over 140 dB for each value of θ and this temperature is about 2.5 K, 35 K, and 147 K for $\theta = 180°$, $160°$, and $158°$, respectively. As to IL, it monotonously decreases for $\theta = 180°$ but continuously increases for $\theta = 160°$ and $158°$ as temperature T becomes larger. It is worth noting that we have IL < 1.0 dB in a wide range of temperature T of our interest for $\theta > 160°$ while IL exceeds 1.0 dB at $T = 235$ K for $\theta = 158°$. Anyway, this figure tells that it is viable to attain a better trade-off between IR and IL so as to realize a high-performance optical isolator by simultaneously modulating angle θ and temperature T in appropriate ranges. The main benefit of such a joint modulation lies in that it promises a flexible manipulation on both residual Doppler broadenings of two-photon transitions and inevitable Doppler shifts of effective Rabi

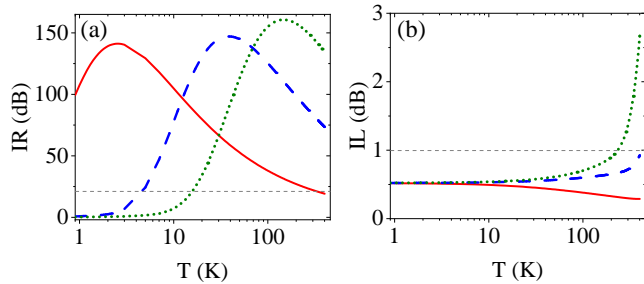frequencies and dynamic Stark shifts.

FIG. 9. Isolation ratio IR (a) and insertion loss IL (b) against temperature T for $\theta = 180°$ (red-solid), $160°$ (blue-dashed), and $158°$ (green-dotted). Relevant parameters are the same as in Fig. 3 except $\Delta_p = -1000$ MHz. Gray dotted lines refer to IR $= 20$ dB in (c) or IL $= 1.0$ dB in (d) as a reference.

V. CONCLUSIONS

In summary, we have investigated an efficient scheme for achieving the magnet-free optical non-reciprocity in a three-level Λ system dominated by two-photon transitions by considering the free-space thermal ^{87}Rb atoms as an example. The forward probe field is found to experience a Doppler-free EIT window and hence suffers very low losses in transmission, while the backward probe field is strongly absorbed because the EIT window is smeared out as the Doppler shifts on two-photon transitions $|1\rangle \leftrightarrow |5\rangle$ and $|2\rangle \leftrightarrow |5\rangle$ don't cancel out again. It is of particular interest that the non-reciprocal transmission may be well controlled by modulating the frequency and amplitude of an assistant field as well as a common misaligned angle between the two pairs of $\{\omega_p, \omega_a\}$ and $\{\omega_{c1}, \omega_{c2}\}$ fields. It is also important that this transmission non-reciprocity can exhibit high isolation ratios and low insertion losses in a wide frequency range, benefiting from largely reduced Doppler broadenings on two-photon transitions $|1\rangle \leftrightarrow |5\rangle$ and $|2\rangle \leftrightarrow |5\rangle$. That means, our scheme allows to manipulate hundreds of probe fields as multiple light signals at the same time with similar isolation ratios and insertion losses due to their insensitivities to single-photon detunings and hence facilitate WDM applications in all-optical networks.

ACKNOWLEDGMENTS

Appendix A: Absorption coefficient

Here, we try to derive the two-photon absorption coefficient of a probe field based on population ρ_{55} in state $|5\rangle$ as the five-level Λ system in Fig. 1(a) reduces to the three-level Λ system in Fig. 1(b). To this end, we first note that the probe field exhibits an intensity defined as $I_p = c\epsilon_0 E_p^2/2 = 2\hbar^2 c\epsilon_0 |\Omega_p|^2/d_{13}^2$. Then, the number of probe photons, passing through a section of the atomic sample at position z, per time is given by

$$\frac{N_p(z)}{dt} = \frac{\pi r_p^2}{\hbar \omega_p} I_p(z) = \frac{\hbar \epsilon_0 \lambda_p r_p^2}{d_{13}^2} |\Omega_p(z)|^2, \quad \text{(A1)}$$

where r_p denotes the probe beam radius. With this consideration, we can further attain the number of photons lost per time in an atomic slice from z to $z + dz$

$$\frac{dN_p}{dt} = \frac{\hbar c\epsilon_0 \lambda_p r_p^2}{d_{13}^2} dI_p, \quad \text{(A2)}$$

with $dN_p = N_p(z+dz) - N_p(z)$ and $dI_p = |\Omega_p(z+dz)|^2 - |\Omega_p(z)|^2$. Meanwhile, the number of atoms in state $|5\rangle$ lost per time, due to spontaneous decay after absorbing probe photons, in this atomic slice is given by

$$\frac{\delta n_a}{dt} = N \pi r_p^2 \rho_{55} \Gamma dz, \quad \text{(A3)}$$

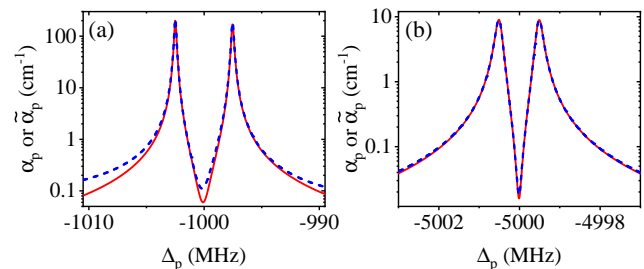where we have considered that the probe field interacts with $N\pi r_p^2 dz$ atoms in this slice of density N.

FIG. 10. Absorption coefficients α_p (red-solid) and $\tilde{\alpha}_p$ (blue-dashed) as functions of probe detuning Δ_p with $\Delta_a = \Delta_{c1} = 1000$ MHz (a) and $\Delta_a = \Delta_{c1} = 5000$ MHz (b). Other parameters are the same as in Fig. 2 except $\Omega_a = 50$ MHz and $\Delta_{c2} = -\Delta_{c1} - \Delta_{5d} + \Delta_{2d}$ changes with $\Delta_a = \Delta_{c1}$.

According to the requirement of energy conservation $dN_p/dt = -\delta n_a/dt$, we can derive the probe transmissivity for an atomic sample of length L

$$T_p = \frac{I_p(L)}{I_p(0)} = \left| \frac{\Omega_p(L)}{\Omega_p(0)} \right|^2 = e^{-\alpha_p L}, \quad \text{(A4)}$$

with the absorption coefficient being

$$\alpha_p = \frac{N d_{13}^2}{\hbar \epsilon_0} \frac{\pi \Gamma}{\lambda_p} \frac{\rho_{55}}{|\Omega_p|^2}, \quad \text{(A5)}$$

which should be Ω_p-independent since $\rho_{55} \propto |\Omega_p|^2$ in the limit of a weak probe field. It is worth noting that the absorption coefficient may also be expressed as

$$\tilde{\alpha}_p = \frac{N d_{13}^2}{\hbar \epsilon_0} \frac{2\pi}{\lambda_p} \frac{\text{Im}\rho_{31}}{\Omega_p}, \quad \text{(A6)}$$

with $\rho_{31} \propto \Omega_p$ obtained by solving density matrix equations of the original five-level Λ system in the steady state. Equations (A5) and (A6) allow us to examine the validity of a reduced three-level Λ system by presenting a numerical comparison between the two absorption coeffi-

cients with appropriate parameters as shown in Fig. 10. The results tell that absorption coefficients α_p and $\tilde{\alpha}_p$ are in good agreement for $|\Delta_{a,c1,c2}|/\Omega_{a,c1,c2} = 20$ and fit better for $|\Delta_{a,c1,c2}|/\Omega_{a,c1,c2} = 100$ in the case of two-photon near resonances $\Delta_p \simeq -\Delta_a$ and $\Delta_{c1} \simeq -\Delta_{c2}$.

[1] L. F. Liu, Y. Zhang, S. C. Zhang, J. Qian, S. Q. Gong, and Y. P. Niu, Magnetic-free unidirectional polarization rotation and free-space optical isolators and circulators, Appl. Phys. Lett. **121**, 261102 (2022).

[2] K. Xia, F. Nori, and M. Xiao, Cavity-free optical isolators and circulators using a chiral cross-Kerr nonlinearity, Phys. Rev. Lett. **121**, 203602 (2018).

[3] K. Xia, G. Lu, G. Lin, Y. Cheng, Y. Niu, S. Gong, and J. Twamley, Reversible nonmagnetic single-photon isolation using unbalanced quantum coupling, Phys. Rev. A **90**, 043802 (2014).

[4] D. Jalas, A. Petrov, M. Eich, W. Freude, S. Fan, Z. Yu, R. Baets, M. Popović, A. Melloni, J. D. Joannopoulos, M. Vanwolleghem, C. R. Doerr, and H. Renner, What is - and what is not - an optical isolator, Nat. Photonics **7**, 579 (2013).

[5] L. Bi, J. Hu, P. Jiang, D. H. Kim, G. F. Dionne, L. C. Kimerling, and C. A. Ross, On-chip optical isolation in monolithically integrated non-reciprocal optical resonators, Nat. Photonics **5**, 758 (2011).

[6] A. B. Khanikaev, S. H. Mousavi, G. Shvets, and Y. S. Kivshar, One-way extraordinary optical transmission and nonreciprocal spoof plasmons, Phys. Rev. Lett. **105**, 126804 (2010).

[7] C. Caloz, A. Alù, S. Tretyakov, D. Sounas, K. Achouri, and Z.-L. Deck-Léger, Electromagnetic nonreciprocity, Phys. Rev. Appl. **10**, 047001 (2018).

[8] L. D. Bino, J. M. Silver, M. T. M. Woodley, S. L. Stebbings, X. Zhao, and P. Del'Haye, Microresonator isolators and circulators based on the intrinsic nonreciprocity of the Kerr effect, Optica **5**, 279 (2018).

[9] A. B. Khanikaev and A. Alù, Nonlinear dynamic reciprocity, Nat. Photonics **9**, 359 (2015).

[10] D. L. Sounas, J. Soric, and A. Alù, Broadband passive isolators based on coupled nonlinear resonances, National Electron. Rev. **1**, 113 (2018).

[11] B. Peng, S. K. Özdemir, F. Lei, F. Monifi, M. Gianfreda, G. L. Long, S. Fan, F. Nori, C. M. Bender, and L. Yang, Parity-time-symmetric whispering-gallery microcavities, Nat. Phys. **10**, 394 (2014).

[12] L. Fan, J. Wang, L. T. Varghese, H. Shen, B. Niu, Y. Xuan, A. M. Weiner, and M. Qi, An all-silicon passive optical diode, Science **335**, 447 (2012).

[13] L. Chang, X. Jiang, S. Hua, C. Yang, J. Wen, L. Jiang, G. Wang, G. Li, and M. Xiao, Parity-time symmetry and variable optical isolation in active-passive-coupled microresonators, Nat. Photonics **8**, 524 (2014).

[14] N. Bender, S. Factor, J. D. Bodyfelt, H. Ramezani, D. N. Christodoulides, F. M. Ellis, and T. Kottos, Observation of asymmetric transport in structures with active nonlinearities, Phys. Rev. Lett. **110**, 234101 (2013).

[15] A. Muñoz de las Heras, and I. Carusotto, Optical isolators based on nonreciprocal four-wave mixing, Phys. Rev. A **106**, 063523 (2022).

[16] M. Han, Y. He, Q. Li, X. Song, Y. Wang, A. Yang, Q. Zeng, and Y. Peng, Efficient optical isolator via dual-Raman process with chiral nonlinearity, Results Phys. **46**, 106288 (2023).

[17] A. Graf, S. D. Rogers, J. Staffa, U. A. Javid, D. H. Griffith, and Q. Lin, Nonreciprocity in photon pair correlations of classically reciprocal systems, Phys. Rev. Lett. 128, 213605 (2022).

[18] D. L. Sounas and A. Alù, Non-reciprocal photonics based on time modulation, Nat. Photonics **11**, 774 (2017).

[19] Z. Yu and S. Fan, Complete optical isolation created by indirect interband photonic transitions, Nat. Photonics **3**, 91 (2009).

[20] D. L. Sounas and A. Alù, Angular-momentum-biased nanorings to realize magnetic-free integrated optical isolation, ACS Photonics **1**, 198 (2014).

[21] N. A. Estep, D. L. Sounas, J. Soric, and A. Alù, Magnetic-free non-reciprocity and isolation based on parametrically modulated coupled-resonator loops, Nat. Phys. **10**, 923 (2014).

[22] M. S. Kang, A. Butsch and P. S. J. Russell, Reconfigurable light-driven opto-acoustic isolators in photonic crystal fibre, Nat. Photonics **5**, 549 (2011).

[23] Z. Shen, Y.-L. Zhang, Y. Chen, C.-L. Zou, Y.-F. Xiao, X.-B. Zou, F.-W. Sun, G.-C. Guo, and C.-H. Dong, Experimental realization of optomechanically induced nonreciprocity, Nat. Photonics **10**, 657 (2016).

[24] H. Xu, L. Jiang, A. A. Clerk, and J. G. E. Harris, Nonreciprocal control and cooling of phonon modes in an optomechanical system, Nature **568**, 65 (2019).

[25] F. Ruesink, J. P. Mathew, M. A. Miri, A. Alù, and E. Verhagen, Optical circulation in a multimode optomechanical resonator, Nat. Commun. **9**, 1798 (2018).

[26] F. Ruesink, M. A. Miri, A. Alù, and E. Verhagen, Nonreciprocity and magnetic-free isolation based on optomechanical interactions, Nat. Commun. **7**, 13662 (2016).

[27] Z. Shen, Y. L. Zhang, Y. Chen, F. W. Sun, X. B. Zou, G. C. Guo, C. L. Zou, and C. H. Dong, Reconfigurable optomechanical circulator and directional amplifier, Nat. Commun. **9**, 1797 (2018).

[28] K. Fang, J. Luo, A. Metelmann, M. H. Matheny, F. Marquardt, A. A. Clerk, and O. Painter, Generalized nonreciprocity in an optomechanical circuit via synthetic magnetism and reservoir engineering, Nat. Phys. **13**, 465 (2017).

[29] S. A. R. Horsley, J.-H. Wu, M. Artoni, and G. C. La Rocca, Optical nonreciprocity of cold atom Bragg mirrors in motion, Phys. Rev. Lett. **110**, 223602 (2013).

[30] L. Yang, Y. Zhang, X.-B. Yan, Y. Sheng, C.-L. Cui, and J.-H. Wu, Dynamically induced two-color nonreciprocity in a tripod system of a moving atomic lattice, Phys. Rev. A. **92**, 053859 (2015).

[31] D. W. Wang, H. T. Zhou, M. J. Guo, J. X. Zhang, J. Evers, and S. Y. Zhu, Optical diode made from a moving

photonic crystal, Phys. Rev. Lett. **110**, 093901 (2013).

[32] Y. Tang, and A. E. Cohen, Optical chirality and its interaction with matter, Phys. Rev. Lett. **104**, 163901 (2010).

[33] T. Li, A. Miranowicz, X. Hu, K. Xia, and F. Nori, Quantum memory and gates using a Lambda-type quantum emitter coupled to a chiral waveguide, Phys. Rev. A **97**, 062318 (2018).

[34] P. Lodahl, S. Mahmoodian, S. Stobbe, A. Rauschenbeutel, P. Schneeweiss, J. Volz, H. Pichler, and P. Zoller, Chiral quantum optics, Nature **541**, 473 (2017).

[35] C. Sayrin, C. Junge, R. Mitsch, B. Albrecht, D. O'Shea, P. Schneeweiss, J. Volz, and A. Rauschenbeutel, Nanophotonic optical isolator controlled by the internal state of cold atoms, Phys. Rev. X **5**, 041036 (2015).

[36] M. Scheucher, A. Hilico, E.Will, J. Volz, and A. Rauschenbeutel, Quantum optical circulator controlled by a single chirally coupled atom, Science **354**, 1577 (2016).

[37] S. Zhang, Y. Hu, G. Lin, Y. Niu, K. Xia, J. Gong, and S. Gong, Thermal-motion-induced non-reciprocal quantum optical system, Nat. Photonics **12**, 744 (2018).

[38] Y. Q. Hu, S. C. Zhang, and Y. H. Qi, Multiwavelength magnetic-free optical isolator by optical pumping in warm atoms, Phys. Rev. Appl. **12**, 054004 (2019).

[39] S. Zhang, G. Lin, Y. Hu, Y. Qi, Y. Niu, and S. Gong, Cavity-free circulator with low insertion loss using hot atoms, Phys. Rev. Appl. **14**, 024032 (2020).

[40] G. Lin, S. Zhang, Y. Hu, Y. Niu, J. Gong, and S. Gong, Nonreciprocal amplification with four-level hot atoms, Phys. Rev. Lett. **123**, 033902 (2019).

[41] E.-Z. Li, D.-S. Ding, Y.-C. Yu, M.-X. Dong, L. Zeng, W.-H. Zhang, Y.-H. Ye, H.-Z. Wu, Z.-H. Zhu, W. Gao, G.-C. Guo, and B.-S. Shi, Experimental demonstration of cavity-free optical isolators and optical circulators, Phys. Rev. Research **2**, 033517 (2020).

[42] C. Liang, B. Liu, A.-N. Xu, X. Wen, C. Lu, K. Xia, M. K. Tey, Y.-C. Liu, and L. You, Collision-induced broadband optical nonreciprocity, Phys. Rev. Lett. **125**, 123901 (2020).

[43] S. Zhang, Y. Zhan, S. Gong, and Y. Niu, Noiseless single-photon isolator at room temperature, Commun. Phys. **6**, 33 (2023).

[44] C. Li, Q. Yu, Y. Zhang, M. Xiao, and Z. Zhang, Optical isolation with optical parametric amplification in an atomic system, Laser Photonics Rev. **17** 2200267 (2023).

[45] F. Song, Z. P. Wang, E. Z. Li, B. L. Yu, and Z. X. Huang, Nonreciprocity with structured light using optical pumping in hot atoms, Phys. Rev. Appl. **18**, 024027 (2022).

[46] M.-X. Dong, K.-Y. Xia, W.-H. Zhang, Y.-C. Yu, Y.-H. Ye, E.-Z. Li, L. Zeng, D.-S. Ding, B.-S. Shi, G.-C. Guo, and F. Nori, All-optical reversible single-photon isolation at room temperature, Sci. Adv. **7**, eabe8924 (2021).

[47] K.-Y. Liao, H.-T. Tu, S.-Z. Yang, C.-J. Chen, X.-H. Liu, J. Liang, X.-D. Zhang, H. Yan, and S.-L. Zhu, Microwave electrometry via electromagnetically induced absorption in cold Rydberg atoms, Phys. Rev. A **101**, 053432 (2020).

[48] D. Yan, J.-W. Gao, Q.-Q. Bao, H. Yang, H. Wang, and J.-H. Wu, Electromagnetically induced transparency in a five-level Λ system dominated by two-photon resonant transitions, Phys. Rev. A **83**, 033830 (2011).

[49] D. J. Richardson, J. M. Fini, and L. E. Nelson, Space-division multiplexing in optical fibres, Nat. Photonics **7**, 354 (2013).

[50] A. Pasquazi, M. Peccianti, L. Razzari, D. J. Moss, S. Coen, M. Erkintalo, Y. K. Chembo, T. Hansson, S. Wabnitz, P. Del'Haye, X. Xue, A. M. Weiner, and R. Morandotti, Micro-combs: A novel generation of optical sources, Phys. Rep. **729**, 1 (2018).

[51] Y. Doi, T. Yoshimatsu, Y. Nakanishi, S. Tsunashima, M. Nada, S. Kamei, K. Sano, and Y. Ishii, Receiver integration with arrayed waveguide gratings toward multi-wavelength data-centric communications and computing, Appl. Sci. **10**, 8205 (2020).

[52] E. A. Kittlaus, N. T. Otterstrom, P. Kharel, S. Gertler, and P. T. Rakich, Non-reciprocal interband Brillouin modulation, Nat. Photonics **12**, 613 (2018).

[53] W.-B. Yan, W.-Y. Ni, J. Zhang, F.-Y. Zhang, and H. Fan, Tunable single-photon diode by chiral quantum physics, Phys. Rev. A **98**, 043852 (2018).

[54] C. Fan, F. Shi, H. Wu, and Y. Chen, Tunable all-optical plasmonic diode based on Fano resonance in nonlinear waveguide coupled with cavities, Opt. Lett. **40**, 2449 (2015).

[55] S. Fan, Y. Qi, G. Lin, Y. Niu, and S. Gong, Broadband optical nonreciprocity in an N-type thermal atomic system, Opt. Commun. **462**, 125343 (2020).

[56] Y.-D. Hu and G.-Q. Zhang, Multichannel nonreciprocal amplifications using cesium vapor, Phys. Rev. A **107**, 053716 (2023).

[57] S. Fan, Y. Qi, Y. Niu, and S. Gong. Nonreciprocal transmission of multi-band optical signals in thermal atomic systems, Chin. Opt. Lett. **20**, 012701 (2022).

[58] M. O. Scully and M. S. Zubairy, Quantum Optics, Cambridge University Press (1997).

[59] D. A. Steck, Alkali D line data, available online at http://steck.us/alkalidata.

[60] N. Sibalic, J. D. Pritchard, C. S. Adams, and K. J. Weatherill, An introduction to Rydberg atoms with ARC, available online at https://arc-alkali-rydberg-calculator.readthedocs.io/en/latest/Rydberg_atoms_a_primer_notebook.html.